Structural and Magnetic Properties of $[Ni_4(\mu_3\text{-}OMe)_4(dbm)_4(MeOH)_4]$ and $[Ni_4(\eta^1,\mu_3\text{-}N_3)_4(dbm)_4(EtOH)_4]$. Magnetostructural Correlations for $[Ni_4X_4]^{4+}$ Cubane Complexes

Malcolm A. Halcrow, Jui-Sui Sun,† John C. Huffman, and George Christou*

Department of Chemistry and Molecular Structure Center, Indiana University, Bloomington, Indiana 47405-4001

Received March 10, 1995[⊗]

Reaction of $Ni(O_2CMe)_2{\cdot}4H_2O$ with 1 molar equiv of Na(dbm) (dbmH = dibenzoylmethane) and NaOH in refluxing MeOH affords a green precipitate of $[Ni_4(OMe)_4(dbm)_4(MeOH)_4]$ (**1**), which can be recrystallized from chlorinated solvents; recrystallized yield 70%. Crystals of $\mathbf{1}{\cdot}2CH_2Cl_2$ have the following cell parameters at −111 °C: triclinic, $P\bar{1}$, $a = 14.566(2)$, $b = 20.661(4)$, $c = 13.367(2)$ Å; $\alpha = 92.58(1)$, $\beta = 117.17(1)$, $\gamma = 72.87(1)°$; $V = 3433.2$ Å^3; $Z = 2$. The structure was solved and refined by employing 4631 reflections with $F > 2.33\sigma(F)$ to final values of R (R_w) of 6.00% (5.21%). The molecule consists of a $[Ni_4(OMe)_4]^{4+}$ cubane, each Ni^{II} ion being bound to three μ_3-OMe^- ions, one chelating dbm^- group, and one terminal MeOH. Intramolecular hydrogen bonding between the MeOH and dbm^- ligands leads to a distortion of the $[Ni_4(OMe)_4]^{4+}$ core from T_d to D_{2d} symmetry, resulting in two types of Ni_2O_2 faces within the cubane structure with differing Ni··Ni distances, Ni−O−Ni angles, and Ni−O−O−Ni dihedral angles. Reaction of a 1:1:1 molar ratio of $Ni(ClO_4)_2{\cdot}6H_2O$, NaN_3, and Na(dbm) in EtOH at room temperature gives a green precipitate, which affords deep green crystals of $[Ni_4(N_3)_4(dbm)_4(EtOH)_4]$ (**3**) in 78% yield upon recrystallization from chlorinated solvents; similar reactions in MeOH yield products in which MeO^- has been partially substituted for N_3^-. Crystals of $\mathbf{3}{\cdot}2C_7H_8$ have the following cell parameters at −174 °C: monoclinic, $P2_1/n$; $a = 14.295(2)$, $b = 23.203(4)$, $c = 24.542(4)$ Å; $\beta = 100.49(1)°$; $V = 8004.2$ Å^3; $Z = 4$. The structure was solved and refined by employing 6163 reflections with $F > 2.33\sigma(F)$ to final values of R (R_w) = 5.12% (4.44%). The molecule consists of a $[Ni_4(N_3)_4]^{4+}$ cubane, each Ni^{II} ion being bound to three (η^1,μ_3-N_3^-) ligands, one chelating dbm^- and one terminal EtOH. The disposition of ligands about the Ni^{II} ions and structural distortions caused by EtOH···dbm^- hydrogen bonding in **3** are identical to those of **1**. The ^{1}H NMR, UV/visible, and (for **3**) IR spectroscopic properties of **1** and **3** are consistent with octahedrally-coordinated Ni^{II} and strongly suggest that the $[Ni_4(X)_4(dbm)_4(L)_4]$ ($X^- = MeO^-$, N_3^-; L = alcohol, solvent) structure is retained in chlorinated solvents. Both **1** and **3** show only irreversible processes by cyclic voltammetry in CH_2Cl_2/0.5 M $Bu^n_4NClO_4$ at 293 K. The solid-state variable-temperature effective magnetic moment (5.00−320 K) of **1** is modeled by a two-J equation giving $J_1 = -3.4$ cm^{-1}, $J_2 = +12.2$ cm^{-1}, $g = 2.05$, and $\Theta = +2.1$ K ($\mathbf{H} = -2JS_1{\cdot}S_2$). This is in agreement with the observed D_{2d} symmetry of the $[Ni_4(OMe)_4]^{4+}$ core in **1**; a plot of J *vs* Ni−O−Ni bridging angle for **1** and other $[Ni_4(OR)_4]^{4+}$ cubanes shows an excellent linear correlation. By contrast, the variable-temperature magnetic behavior of **3** is well described by a one-J model in which all Ni···Ni interactions are equivalent, with $J = +11.9$ cm^{-1}, $g = 2.05$, and $\Theta = +3.0$ K, despite the observed D_{2d} symmetry of the $[Ni_4(N_3)_4]^{4+}$ core. This result is in agreement with literature data for complexes bridged by a planar $[Ni_2(\eta^1,\mu\text{-}N_3)_2]^{2+}$ group, which show no obvious correlation between J and Ni−N−Ni angle.

We have a longstanding interest in manganese carboxylate aggregates and their relevance as models for the Mn_4 cluster in the photosynthetic water oxidation center (WOC) of green plants and cyanobacteria.[1] During this study, we have prepared several $Mn^{IV}Mn^{III}_3$ complexes containing the distorted cubane $[Mn_4O_3X]^{6+}$ core (X^- = halide, carboxylate)[2] and the cubane $[Co_4O_4]^{4+}$ core,[3] together with protonated versions of the latter.[4] As an extension to this work, we recently turned our attention to cubane complexes containing other metal ions, to further investigate the electronic and magnetic properties of this interesting class of compounds. We recently communicated the structure and magnetic behavior of the novel cubane complex $[Ni_4(N_3)_4(dbm)_4(EtOH)_4]$ (**3**; dbmH = dibenzoylmethane),[5] the first paramagnetic molecule containing end-on, triply-bridging azide ligands.[6-8] We describe here the full characterization of

† Department of Chemistry, Michigan State University, East Lansing, MI 48824-1322.

⊗ Abstract published in *Advance ACS Abstracts,* July 1, 1995.

(1) Christou, G. *Acc. Chem. Res.* **1989**, *22*, 328.
(2) (a) Hendrickson, D. N.; Christou, G.; Schmitt, E. A.; Libby, E.; Bashkin, J. S.; Wang, S.; Tsai, H.-L.; Vincent, J. B.; Boyd, P. D. W.; Huffman, J. C.; Folting, K.; Li, Q.; Streib, W. E. *J. Am. Chem. Soc.* **1992**, *114*, 2455. (b) Wang, S.; Tsai, H.-L.; Streib, W. E.; Christou, G.; Hendrickson, D. N. *J. Chem. Soc., Chem. Commun.* **1992**, 1427. (c) Wemple, M. W.; Tsai, H.-L.; Folting, K.; Hendrickson, D. N.; Christou, G. *Inorg. Chem.* **1993**, *32*, 2025. (d) Wang, S.; Tsai, H.-L.; Hagen, K. S.; Hendrickson, D. N.; Christou, G. *J. Am. Chem. Soc.* **1994**, *116*, 8376.
(3) Dimitrou, K.; Folting, K.; Streib, W. E.; Christou, G. *J. Am. Chem. Soc.* **1993**, *115*, 6432.
(4) Dimitrou, K.; Folting, K.; Streib, W. E.; Christou, G. *J. Chem. Soc., Chem. Commun.* **1994**, 1385.
(5) Halcrow, M. A.; Huffman, J. C.; Christou, G. *Angew. Chem., Int. Ed. Engl.* **1995**, *34*, 889.
(6) (a) Dori, Z.; Ziolo, R. F. *Chem. Rev.* **1973**, *73*, 247. (b) Müller, U. *Struct. Bonding (Berlin)* **1973**, *14*, 141. (c) Vrieze, K.; van Koten, G. In *Comprehensive Coordination Chemistry*; Wilkinson, G., Gillard, R. D., McCleverty, J. A., Eds.; Pergamon: Oxford, U.K., **1987**; Vol. 2, Chapter 13.5, pp 225−236.
(7) (a) von Dahlen, K.-H.; Lorberth, J. *J. Organomet. Chem.* **1974**, *65*, 267. (b) Atam, M.; Müller, U. *Ibid.* **1974**, *71*, 435.
(8) (a) Goher, M. A. S.; Mak, T. C. W. *Inorg. Chim. Acta* **1985**, *99*, 223. (b) Mautner, F. A.; Krischner, H.; Kratky, C. *Z. Kristallogr.* **1985**, *172*, 291. (c) Gross, M. E.; Siegrist, T. *Inorg. Chem.* **1992**, *31*, 4898.

0020-1669/95/1334-4167$09.00/0

3, and present a comparison of its structural, spectroscopic, and magnetochemical properties with those of the analogous methoxide-containing complex $[Ni_4(OMe)_4(dbm)_4(MeOH)_4]$ (**1**).

The structural and magnetochemical properties of several $[Ni_4(OR)_4]^{4+}$ (R = H, alkyl) cubanes have now been reported,[9-14] in most cases the symmetry of the magnetic model employed (i.e., one-*J* or two-*J*) reflecting the effective symmetry (i.e., T_d or D_{2d}) within the $[Ni_4(OR)_4]^{4+}$ cubane core in the solid-state structures of these compounds. The magnetic behavior of **3** contrasts with this observation, however, being well described by a one-*J* equation (T_d symmetry) despite signficant structural distortions and effective D_{2d} symmetry within the $[Ni_4(N_3)_4]^{4+}$ unit of this compound.[5] The mechanisms of transmission of the observed, generally ferromagnetic exchange interactions between paramagnetic metal ions mediated by end-on azide bridges are the topic of continuing discussion. In particular, a recent study of Cu^{II} complexes has suggested that end-on azide bridges should exhibit a marked dependence on Cu−N−Cu bridging angle[15] and show antiferromagnetic interactions for Cu−N−Cu > 108.5°, mirroring the behavior of analogous hydroxide-bridged species and supporting an earlier theoretical study.[16] In contrast, an alternative model of spin polarization in end-on bridging azide ligands has also been described,[17] which predicts ferromagnetic coupling through end-on bridging azide ligands for all Cu−N−Cu angles. We were therefore interested to compare and contrast the magnetostructural properties of Ni^{II} complexes bridged by alkoxide/hydroxide or end-on azide ions, to attempt to understand the different magnetic properties of **1**, which does show D_{2d} magnetic symmetry, and **3**, which does not.

Experimental Section

Syntheses. All manipulations were performed under aerobic conditions. $[Ni_4(OMe)_4(acac)_4(MeOH)_4]$[11] was prepared by the literature procedures; all solvents, $Ni(O_2CMe)_2{\cdot}4H_2O$ (Mallinckrodt), $Ni(ClO_4)_2{\cdot}6H_2O$, and dibenzoylmethane (dbmH; Aldrich) were used as received. **CAUTION:** Complexes containing perchlorate or azide ions are potentially explosive. Handling of only small quantities and the use of appropriate caution are advised.

Na(dbm). Solutions of dbmH (20 g, 89 mmol) in MeCN (200 cm^3) and of NaOH (3.6 g, 89 mmol) in MeOH (150 cm^3) were combined, and the mixture was heated to reflux for 15 min. The resultant yellow solution was then concentrated *in vacuo* until crystals began forming. Storage of the solution at −10 °C for 24 h afforded white needles, which were filtered off and washed with cold MeOH. Further concentration of the filtrate and washings and storage at −10 °C gave a second crop of crystals; total yield 80%. The white crystalline product becomes yellow on drying. Anal. Calcd (found) for $C_{15}H_{11}O_2Na$: C, 73.2 (72.5); H, 4.50 (4.61). Selected IR data (Nujol mull, cm^{-1}): 1553 (s), 1462 (s), 1416 (s), 1343 (m), 1306 (m), 1250 (m), 1165 (m), 1156 (m), 1051 (m), 1028 (s), 1016 (m), 871 (br), 817 (w), 774 (s), 734 (s), 662 (s), 417 (m). Electronic spectrum in MeCN [λ_{max}, nm (ϵ_M, $dm^3{\cdot}mol^{-1}{\cdot}cm^{-1}$)]: 204 (18 450), 238 (11 960), 352 (19 080). ^1H NMR spectrum (CD_3CN), δ, ppm: 7.86 (m, 2H), 7.35 (m, 3H), 6.40 (s, 1H).

$[Ni_4(OMe)_4(dbm)_4(MeOH)_4]$ (1). A mixture of $Ni(O_2CMe)_2{\cdot}4H_2O$ (1.2 g, 4.9 mmol), NaOH (0.20 g, 4.9 mmol), and Na(dbm) (1.2 g, 4.9 mmol) in MeOH (50 cm^3) was refluxed for 30 min, affording a yellow-green precipitate, which was filtered off and washed with MeOH. Recrystallization from CH_2Cl_2/MeOH affords deep green crystals, which are of X-ray quality but lose solvent when removed from their mother liquor; yield 70%. Anal. Calcd (found) for $C_{68}H_{72}O_{16}Ni_4$: C, 59.2 (58.9); H, 5.26 (5.24); Ni, 17.0 (16.9). Selected IR data (Nujol mull, cm^{-1}): 3200 (br), 1601 (s), 1561 (s), 1512 (s), 1456 (s), 1408 (s), 1309 (m), 1280 (m), 1226 (m), 1045 (s), 1028 (m), 1001 (w), 941 (m), 785 (m), 756 (m), 738 (m), 722 (s), 689 (m), 630 (m), 524 (m), 446 (s). Electronic spectrum in $CHCl_3$ [λ_{max}, nm (ϵ)]: 250 (62 160), 314 (sh), 363 (64 560), 420 (sh), 638 (28). ^1H NMR spectrum ($CDCl_3$), δ, ppm: 293.3, 42.1, 10.6 (sh), 10.1, 8.3, −11.0.

$[Ni(dbm)(py)_4](ClO_4)$ (2). A mixture of $Ni(ClO_4)_2{\cdot}6H_2O$ (1.8 g, 4.9 mmol) and Na(dbm) (1.2 g, 4.9 mmol) in MeOH (50 cm^3) and pyridine (5 cm^3) was refluxed for 1 h, affording a dark green solution, which was evaporated to dryness. Extraction of the green residue into CH_2Cl_2 (50 cm^3) gave a dark green solution, which was filtered, concentrated to 15 cm^3, and layered with hexanes to give large dark green plates together with a small amount of blue powder, which was removed by decantation; yield 55%. Anal. Calcd (found) for $C_{35}H_{31}N_4O_6ClNi$: C, 60.2 (60.2); H, 4.48 (4.55); N, 8.03 (8.02). Selected IR data (Nujol mull, cm^{-1}): 1601 (s), 1555 (s), 1520 (s), 1485 (m), 1476 (s), 1456 (s), 1445 (s), 1402 (s), 1354 (m), 1311 (m), 1280 (w), 1234 (m), 1213 (m), 1156 (m), 1099 (vs), 1069 (w), 1040 (m), 1011 (m), 756 (s), 716 (m), 706 (s), 682 (m), 623 (s), 519 (m), 430 (m). Electronic spectrum in $CHCl_3$ [λ_{max}, nm (ϵ)]: 257 (21470), 278 (sh), 359 (27720), 454 (sh), 597 (30.3). ^1H NMR spectrum ($CDCl_3$), δ, ppm: 35.8, 14.6, 10.6, 9.1, 7.8, −14.3.

$[Ni_4(N_3)_4(dbm)_4(EtOH)_4]$ (3). Solid NaN_3 (0.30 g, 4.9 mmol) and Na(dbm) (1.2 g, 4.9 mmol) were added to a solution of $Ni(ClO_4)_2{\cdot}6H_2O$ (1.8 g, 4.9 mmol) in EtOH (100 cm^3), and the mixture was stirred at room temperature for 4 h. The resultant green precipitate was filtered off, washed with EtOH, and dried in air. Recrystallization from CH_2Cl_2/EtOH afforded deep green blocks which rapidly lose solvent when removed from their mother liquor; yield 78%. Crystallization from toluene/EtOH gave a lower yield of crystals suitable for an X-ray diffraction study. Anal. Calcd (found) for $C_{68}H_{68}N_{12}O_{12}Ni_4$: C, 55.2 (54.4); H, 4.63 (4.65); N, 11.4 (11.4); Ni, 15.9 (16.1). Selected IR data (Nujol mull, cm^{-1}): 3270 (br), 2087 (vs), 1595 (s), 1554 (s), 1516 (s), 1454 (m), 1402 (m), 1383 (s), 1312 (s), 1292 (m), 1242 (m), 1229 (w), 1057 (m), 1047 (m), 1024 (m), 941 (m), 754 (m), 725 (s), 691 (m), 637 (m), 530 (m). IR spectrum ($CHCl_3$, cm^{-1}): 2089. Electronic spectrum in $CHCl_3$ [λ_{max}, nm (ϵ)]: 246 (sh), 258 (85 520), 280 (sh), 364 (77 610), 412 (sh), 652 (41). ^1H NMR spectrum ($CDCl_3$), δ, ppm: 57.2, 50.4, 12.8, 11.7, 10.2, 9.3, −17.3.

$[Ni(dbm)_2(py)_2]$ (4). A mixture of $Ni(O_2CMe)_2{\cdot}4H_2O$ (1.2 g, 4.9 mmol) and Na(dbm) (2.4 g, 9.8 mmol) in water (100 cm^3) and pyridine (50 cm^3) was refluxed for 8 h, giving a mustard-colored precipitate, which was filtered off, washed with MeOH, and dried in air. Extraction of this solid with CH_2Cl_2 (50 cm^3) yielded a dark brown solution which was filtered, concentrated to 15 cm^3, and layered with hexanes. The product formed dark brown crystals, which were filtered off, washed with hexanes, and dried *in vacuo*; yield 50%. Anal. Calcd (found) for $C_{40}H_{32}N_2O_4Ni$: C, 72.4 (72.6); H, 4.86 (4.95); N, 4.22 (4.18). Selected IR data (Nujol mull, cm^{-1}): 1597 (m), 1553 (m), 1514 (m), 1460 (s), 1420 (m), 1354 (m), 762 (m), 748 (m), 727 (s), 694 (s), 630 (m), 530 (m), 434 (m). Electronic spectrum in $CHCl_3$ [λ_{max}, nm (ϵ)]: 256 (30 270), 300 (sh), 348 (44 100), 364 (sh), 418 (sh), 584 (19.2). ^1H NMR spectrum ($CDCl_3$), δ, ppm: 37.9, 15.1, 10.2, 9.2, 7.4, −12.9.

X-ray Crystallography. Data were collected using a Picker four-circle diffractometer; details of the diffractometry, low-temperature facilities, and computational procedures employed by the Molecular Structure Center are available elsewhere.[18] The structures of complexes **1**·$2CH_2Cl_2$ and **3**·$2C_7H_8$ were determined using a combination of direct

(9) (a) Schrauzer, G. N.; Kohnle, J. *Chem. Ber.* **1964**, *97*, 1727. (b) Krüger, A. G.; Winter, G. *Aust. J. Chem.* **1970**, *23*, 1. (c) Clare, B. W.; Kepert, D. L. *Ibid.* **1975**, *28*, 1489.
(10) (a) Andrew, J. E.; Blake, A. B. *J. Chem. Soc. A* **1969**, 1456. (b) Barnes, J. A.; Hatfield, W. E. *Inorg. Chem.* **1971**, *10*, 2355.
(11) (a) Bertrand, J. A.; Caine, D. *J. Am. Chem. Soc.* **1964**, *86*, 2298. (b) Bertrand, J. A.; Ginsberg, A. P.; Kaplan, R. I.; Kirkwood, C. E.; Martin, R. L.; Sherwood, R. C. *Inorg. Chem.* **1971**, *10*, 240.
(12) (a) Aurivillius, B. *Acta Chem. Scand., Ser. A* **1977**, *31*, 501. (b) Boyd, P. D. W.; Martin, R. L.; Schwarzenbach, G. *Aust. J. Chem.* **1988**, *41*, 1449.
(13) Gladfelter, W. L.; Lynch, M. W.; Schaefer, W. P.; Hendrickson, D. N.; Gray, H. B. *Inorg. Chem.* **1981**, *20*, 2390.
(14) Ballester, L.; Coronado, E.; Gutiérrez, A.; Monge, A.; Perpiñán, M. F.; Pinilla, E.; Rico, T. *Inorg. Chem.* **1992**, *31*, 2053.
(15) Tandon, S. S.; Thompson, L. K.; Manuel, M. E.; Bridson, J. N. *Inorg. Chem.* **1994**, *33*, 5555.
(16) Comarmond, J.; Plumeré, P.; Lehn, J.-M.; Agnus, Y.; Louis, R.; Weiss, R.; Kahn, O.; Morgenstern-Badarau, I. *J. Am. Chem. Soc.* **1982**, *104*, 6330.
(17) Charlot, M.-F.; Kahn, O.; Chaillet, M.; Larrieu, C. *J. Am. Chem. Soc.* **1986**, *108*, 2574.

Table 1. Crystallographic Data for Compound $1{\cdot}2CH_2Cl_2$ and $3{\cdot}2C_7H_8$

	$1{\cdot}2CH_2Cl_2$	$3{\cdot}2C_7H_8$
formula[a]	$C_{70}H_{76}O_{16}Cl_4Ni_4$	$C_{82}H_{84}N_{12}O_{12}Ni_4$
fw[a]	1550.01	1661.46
space group	$P\bar{1}$	$P2_1/n$
a, Å	14.566(2)	14.295(2)
b, Å	20.661(4)	23.203(4)
c, Å	13.367(2)	24.542(4)
α, deg	92.58(1)	xx
β, deg	116.17(1)	100.49(1)
γ, deg	72.87(1)	xx
V, Å^3	3433.24	8004.23
Z	2	4
T, °C	−111	−174
radiation, Å[b]	0.710 69	0.710 69
ϱ_{calc}, g/cm^3	1.50	1.38
μ, cm^{-1}	13.08	9.96
$R(F_o)$[c]	0.0600	0.0512
$R_w(F_o)$[d]	0.0521	0.0444

[a] Including solvate molecules. [b] Graphite monochromator. [c] $R = \sum||F_o| - |F_c||/\sum|F_o|$. [d] $R_w = [\sum w(|F_o| - |F_c|)2/\sum w|F_o|^2]^{1/2}$ where $w = 1/\sigma^2(|F_o|)$.

methods and Fourier techniques (SHELXTL-PC) and refined by full-matrix least-squares cycles.

For compound $1{\cdot}2CH_2Cl_2$, a systematic search of a limited hemisphere of reciprocal space located a set of diffraction maxima with no symmetry or systematic absences, corresponding to one of the triclinic space groups. Subsequent solution and refinement of the structure confirmed the initial choice of the centrosymmetric $P\bar{1}$ to be correct. Data $(+h,\pm k,\pm l)$ were collected to $2\theta = 45°$ and corrected for Lorentz and polarization terms, and equivalent data were averaged. After the non-hydrogen atoms had been located and partially refined, all of the hydrogen atoms were observed in difference Fourier maps phased on the non-hydrogen atoms and were placed in idealized positions as fixed atom contributors in the least-squares treatment; the four hydroxyl hydrogen atoms associated with the methanol ligands were fixed in their located positions. Two of the dbm^- phenyl rings, C(32)−C(37) and C(66)−C(71), show enlarged thermal parameters which may reflect disorder in these groups; this was not modeled, however, because of the relatively low ratio of parameters to observed reflections for this structure. There are two CH_2Cl_2 molecules present in the asymmetric unit, both showing some disorder and partial occupancy. The final difference Fourier map was featureless, the largest peak being 0.43 e/Å^3. Final R and R_w values are included in Table 1.

For compound $3{\cdot}2C_7H_8$, a systematic search of a limited hemisphere of reciprocal space revealed a set of reflections with monoclinic symmetry and systematic absences corresponding to the unique space group $P2_1/n$. Subsequent solution and refinement of the structure confirmed this choice. Data $(+h,+k,\pm l)$ were collected to $2\theta = 45°$ and corrected for Lorentz and polarization terms, and equivalent data were averaged. A difference Fourier map phased on the non-hydrogen atoms clearly located most hydrogen atoms, and all hydrogen atoms were included in the subsequent least-squares refinement in fixed idealized positions; hydrogen atoms attached to the hydroxyl groups of the ethanol ligands were not unambiguously located and were thus omitted from the refinement. Two toluene molecules are present in the cell, both well-ordered. One of the EtOH groups (that beginning with O(20)) has carbon atoms showing large thermal ellipsoids, indicating that the ethyl group here is either highly fluxional or slightly disordered. The final difference Fourier map was essentially featureless. Final R and R_w values are included in Table 1.

Other Measurements. Infrared (Nujol mull, KBr plates) and electronic spectra ($CHCl_3$, 1 cm quartz cell) were recorded on Nicolet 510P (400−4000 cm^{-1}) and Hewlett-Packard 8452A (190−820 nm) spectrophotometers, respectively. NMR spectra were obtained using Varian XL300 (^{1}H, operating at 299.95 MHz) and Nicolet NT360 (^{2}H, 55.42 MHz) spectrometers. Elemental microanalyses were performed by Atlantic Microlab, Norcross, GA, or the microanalytical laboratory of the University of Manchester. Electrochemical measurements were performed in CH_2Cl_2/0.5 M $Bu^n_4NClO_4$ at 293 K using a BAS CV50W voltammetric analyzer, employing a glassy carbon working electrode, a Pt wire auxiliary electrode, and an SCE reference electrode. Potentials are quoted *vs* the ferrocene/ferrocenium couple, which occurs at $E_{1/2}$ = +0.40 V *vs* SCE. Variable-temperature magnetic susceptibility measurements were obtained at Michigan State University with a Quantum Design MPMS SQUID susceptometer operating with a 10 kG (1 T) applied magnetic field. The experimental magnetic susceptibilities were corrected for the diamagnetic response using Pascal's constants.

Results and Discussion

Syntheses and Spectroscopic Characterization. The reaction of $Ni(O_2CMe)_2{\cdot}4H_2O$ with 1 molar equiv of Na(dbm) and NaOH in refluxing MeOH rapidly affords a yellow-green precipitate of analytically pure $[Ni_4(OMe)_4(dbm)_4(MeOH)_4]$ (**1**) in almost quantitative yield, as evidenced by microanalysis and ^{1}H NMR spectroscopy (*vide infra*). Compound **1** is very soluble in chlorinated solvents and toluene, the layering of solutions of **1** in these solvents with MeOH affording large X-ray-quality crystals in 70−80% overall yield. Omission of NaOH from this reaction results in reduced (*ca.* 50%) yields of **1**. Interestingly, attempts to synthesize the known complex $[Ni_4(OMe)_4(acac)_4(MeOH)_4]$ (acacH = 2,4-pentanedione) from $Ni(O_2CMe)_2{\cdot}4H_2O$ and Na(acac) by a similar one-pot reaction were unsuccessful; treatment of $Ni(acac)_2{\cdot}2MeOH$ with NaOH in refluxing MeOH did afford the required product, however, in agreement with the literature procedure.[11] Two attempts were made to synthesize the substituted products $[Ni_4(OMe)_4(dbm)_4(L)_n]^{(4-n)-}$ (L = pyridine, MeCN, $n = 4$; L = $MeCO_2^-$, $n = 2$). First, carrying out the above synthesis in the presence of a stoichiometric amount of pyridine affords **1** as before. If a 1:1 MeOH:pyridine solvent mixture is used, however, a deep green solution results, from which dark green crystals of the octahedral complex $[Ni(dbm)(py)_4](ClO_4)$ (**2**; py = pyridine) can be obtained upon addition of $NaClO_4$ and layering of the solution with Et_2O. Second, recrystallization of **1** from CH_2Cl_2/L (1:1; L = pyridine, MeCN) solvent mixtures and MeOH or from CH_2Cl_2/MeOH in the presence of 2 molar equiv of $Bu^n_4NO_2CMe$ again gives only unchanged **1**; utilization of hexanes as the crystallization solvent in all cases yields only an amorphous powder.

A one-pot reaction of a 1:1:1 molar ratio of $Ni(ClO_4)_2{\cdot}6H_2O$, NaN_3, and Na(dbm) in EtOH at room temperature for 4 h affords a bright green precipitate containing **3** and a little $NaClO_4$. Recrystallization from CH_2Cl_2/EtOH gives large green crystals of pure **3** in 78% overall yield. The IR spectrum of **3** as a Nujol mull contains, in addition to bands arising from dbm^- and coordinated EtOH, a very strong absorption at 2087 cm^{-1} attributable to the ν_{asym}(N−N−N) stretching vibration from coordinated azide;[19] this band appears at 2089 cm^{-1} in $CHCl_3$ solution and is unchanged after standing for 3 days. The ν_{sym}(N−N−N) and δ(N−N−N) vibrations also expected from a metal-bound azide[19] were masked by absorptions from the dbm^- ligand and could not be positively identified, although a shoulder at 541 cm^{-1} which is not present in the spectra of the other compounds in this study may correspond to the latter vibration.

Attempts to synthesize the analogous complex $[Ni_4(N_3)_4(dbm)_4(MeOH)_4]$ by the reaction of $Ni(ClO_4)_2{\cdot}6H_2O$, NaN_3, and Na(dbm) in MeOH or by recrystallization of **3** from CH_2Cl_2/MeOH resulted in partial (up to *ca.* 30%) displacement of N_3^- in the $[Ni_4(N_3)_4]^{4+}$ framework by MeO^- and the isolation of a

(18) Chisholm, M. H.; Folting, K.; Huffman, J. C.; Kirkpatrick, C. C. *Inorg. Chem.* **1984**, *23*, 1021.

(19) Nakamoto, K. *Infrared and Raman Spectra of Inorganic and Coordination Compounds*, 4th ed.; Wiley: New York, 1986.

compound of apparent stoichiometry $[Ni(OMe)_x(N_3)_{1-x}(dbm)(MeOH)]_4$ (x = *ca.* 0.3). This partial substitution of MeO^- for N_3^- in **3** was evidenced by (i) the appearance of a high-energy shoulder at 2108 cm^{-1} on the $\nu_{asym}(N-N-N)$ peak of the IR spectrum of the methanol-containing species, (ii) the observation of additional peaks at $\delta = -13.6$ and -15.3 ppm in the dbm^- *meso*-CH region of the ^1H NMR spectrum and of a peak at $\delta = 291$ ppm in the ^2H NMR spectrum of the product obtained from a reaction carried out in CD_3OD (*vide infra*), and (iii) an X-ray structural determination of crystals of a product obtained from a reaction carried out in MeOH as described above, which showed signs of disorder in the triply bridging ligand positions.[20]

Repeating the synthesis of **3** using the pseudohalide salts NaCN, NaNCO, and KNCS in place of NaN_3 yields only a yellow-green precipitate containing dbm^- and EtOH by IR spectroscopy and analyzing approximately for $[Ni(dbm)_2(EtOH)_x]$ ($x = 1-2$). While we were unable to fully characterize these products because of their insolubility, reaction of $Ni(O_2CMe)_2{\cdot}4H_2O$ and Na(dbm) in a refluxing 2:1 water:pyridine mixture affords the soluble bis(pyridine) adduct $[Ni(dbm)_2(py)_2]$ (**4**) after recrystallization of the resultant precipitate from CH_2Cl_2/hexanes, which shows the IR, NMR, and UV/visible spectroscopic properties expected of a mononuclear octahedral Ni^{II} complex.

The UV/visible and NMR spectroscopic properties of **1** and **3** are similar and will be discussed together. The electronic spectra of both complexes in $CHCl_3$ show a $d-d$ band in the visible region typical of octahedral Ni^{II},[21] at λ_{max} values of 638 nm (ϵ_M = 28 $dm^3{\cdot}mol^{-1}{\cdot}cm^{-1}$ per Ni_4 cubane; **1**) and 652 (41; **3**), together with three higher energy absorptions with λ_{max} values of approximately 254, 300, and 364 nm (65 000−85 000). Importantly, these three latter absorbances are also observed in the spectra of **2** and **4**, showing that they are associated with the dbm^- ligand. In addition, only the position of the central band varies significantly between the spectra of **1**−**4**, occurring at $278 < \lambda_{max} < 314$ nm; the UV/visible spectrum of Na(dbm) in MeCN shows peaks at 238 (11 960) and 352 nm (19 080).[22] Hence, by comparison of these spectra, we tentatively assign the 254 and 364 nm absorptions to dbm^- $\pi \rightarrow \pi^*$ transitions and the 278−314 nm absorption to a Ni $\rightarrow \pi^*(dbm^-)$ charge transfer band.

The ^1H NMR spectrum of **1** in $CDCl_3$ is very simple, showing paramagnetically-shifted peaks consistent with the presence of only one environment for the dbm^-, MeOH, and MeO^- groups (Figure 1a); some of the assignments of these peaks were confirmed by a ^2H NMR study of $[Ni_4(OCD_3)_4(dbm)_4(CD_3OD)_4]$ (**1**-d_{28}, Figure 1b), which was prepared by the reaction of $Ni(O_2CMe)_2{\cdot}4H_2O$ and Na(dbm) in CD_3OD as described above. Four resonances attributable to the dbm^- ligand were observed, at δ 10.6 (sh), 10.1, 8.3, and −11.0 ppm, which were assigned to the phenyl *o*-, *m*-, and *p*-C*H* and the *meso*-C*H* protons,

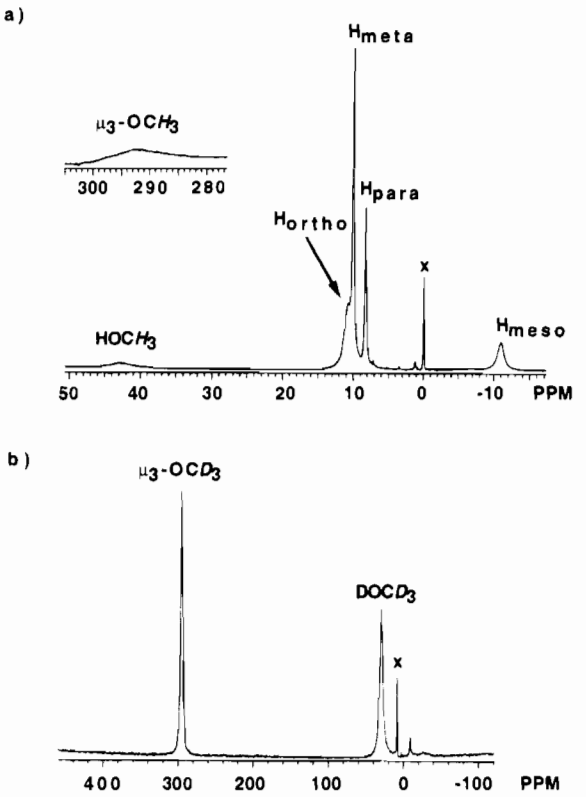

Figure 1. (a) ^1H NMR spectrum of $[Ni_4(OCH_3)_4(dbm)_4(CH_3OH)_4]$ (**1**) in $CDCl_3$. The vertical scale of the inset is 3 times that of the main spectrum. The crossed peak is tetramethylsilane added as a reference. (b) ^2H NMR spectrum of $[Ni_4(OCD_3)_4(dbm)_4(CD_3OD)_4]$ (**1**-d_{28}) in $CHCl_3$. The crossed peak is $CDCl_3$ added as a reference, while the feature at −11 ppm is due to partial deuteration of the dbm^- *meso*-CH protons during the preparation of **1**-d_{28}.

respectively. The resonance from the terminal MeOH methyl protons was broad and appeared at variable positions between 20 and 43 ppm, suggesting that intermolecular exchange of this ligand was occurring; this was confirmed by the addition of CD_3OD to ^1H NMR samples of **1**, or of CH_3OH to ^2H NMR samples of **1**-d_{28}, which led to the rapid (time of mixing) disappearance of this signal. No resonance assignable to the MeOH hydroxyl protons was observable. Finally, a very broad, poorly resolved peak at 290−295 ppm was tentatively assigned to the μ_3-OCH_3 protons. This was confirmed by the deuteration study, the ^2H NMR spectrum of **1**-d_{28} showing a sharp peak at 293.3 ppm (Figure 1b); this ^2H resonance exchanged very slowly upon addition of CH_3OH to the sample, with a half-life of approximately 2 weeks. Complex **3** shows a similar ^1H spectrum in $CDCl_3$, with peaks at δ 57.2, 50.4 (assigned to diastereotopic $HOCH_2CH_3$ protons), 12.8, 11.7, 10.2, 9.3 (dbm^- phenyl *o*-, *m*-, and *p*-C*H* and $HOCH_2CH_3$), and −17.3 ppm (dbm^- *meso*-C*H*). We conclude from these spectra, together with the aforementioned UV/visible and (for **3**) solution IR data, that the $[Ni_4(X)_4(dbm)_4(L)_4]$ ($X^- = MeO^-, N_3^-$; L = alcohol) structures in **1** and **3** are retained in chloroform solution.

The cyclic voltammogram of **1** in CH_2Cl_2/0.5 M $Bu^n_4NClO_4$ at 293 K, scan rate 100 mV/s, shows two irreversible oxidations at $E_{p_a} = +0.75$ and +1.23 V *vs* Fc/Fc^+; the second of these is partially obscured by an additional broad process at $E_{p_a} = +1.4$ V, which may correspond to a dbm^- ligand oxidation. The first oxidation of **1** shows an associated irreversible reduction at $E_{p_c} = -2.10$ V and becomes quasi-reversible at scan rates above 250 mV/s ($E_{1/2} = +0.65$ V, $I_{p_a}/I_{p_c} = 0.4$ at 1 V/s). Addition of 2 molar equiv of $Bu^n_4NO_2CMe$ to the sample causes a cathodic shift in the potentials of the two oxidations, which

(20) $C_{64}H_{60}N_{12}O_{12}Ni_4{\cdot}2CH_2Cl_2$: triclinic, $P\bar{1}$, $a = 14.521(2)$, $b = 20.279(4)$, $c = 13.475(2)$ Å; $\alpha = 92.03(1)$, $\beta = 115.29(1)$, $\gamma = 74.24(1)°$; $V = 3437.8$ Å^3; $Z = 2$. The structure was refined satisfactorily using 5750 reflections with $F > 2.33\sigma(F)$ to R (R_w) values of 5.66% (5.26%). However, examination of the thermal ellipsoids and N−N distances within the azide ligands clearly showed the presence of disorder in these groups, the abnormally small ellipsoids associated with the Ni-bound N atoms in particular being consistent with the partial occupancy of a heavier atom (e.g., O) at these sites. The interpretation of this result as showing partial substitution of MeO^- for N_3^- within the cubane core was subsequently confirmed by the ^2H NMR experiment described in the text.

(21) Sacconi, L.; Mani, F.; Bencini, A. In *Comprehensive Coordination Chemistry*; Wilkinson, G., Gillard, R. D., McCleverty, J. A., Eds.; Pergamon: Oxford, U.K., **1987**; Vol. 5, Chapter 50, pp 45−68.

(22) Eistert, B.; Weygand, F.; Csendes, E. *Chem. Ber.* **1951**, *84*, 745.

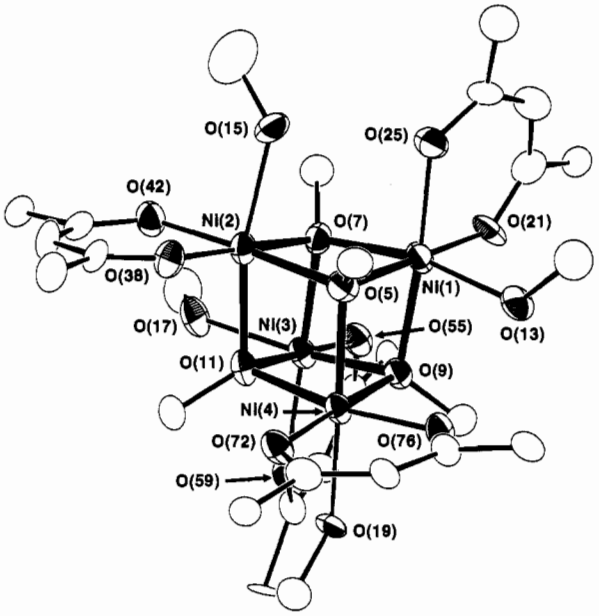

Figure 2. ORTEP representation of $[Ni_4(OMe)_4(dbm)_4(MeOH)_4]$ (**1**). For clarity, only the *ipso* carbon atoms of the dbm^- phenyl groups are shown. The virtual C_2 axis passes through the midpoints of the Ni(2)−Ni(4) and Ni(1)−Ni(3) vectors; the latter are also the two Ni_2 pairs *not* bridged by hydrogen bonds (see text).

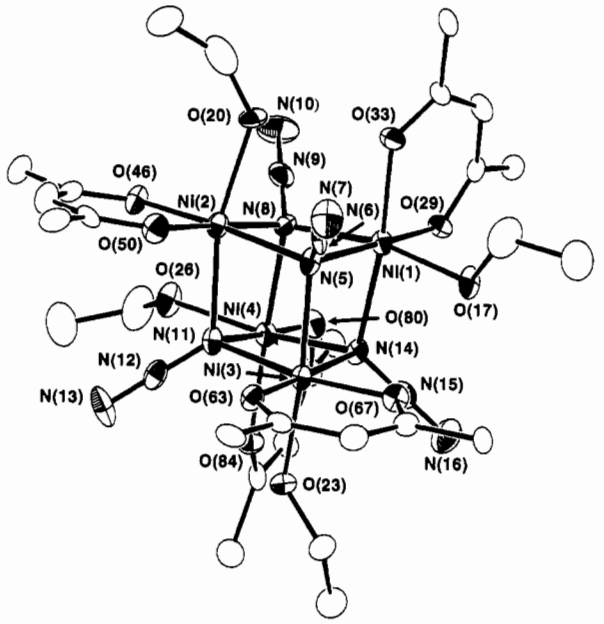

Figure 3. ORTEP representation of $[Ni_4(N_3)_4(dbm)_4(EtOH)_4]$ (**3**). For clarity, only the *ipso* carbon atoms of the dbm^- phenyl groups are shown. The virtual C_2 axis passes through the midpoints of the Ni(2)−Ni(3) and Ni(1)−Ni(4) vectors; the latter are also the two Ni_2 pairs *not* bridged by hydrogen bonds (see text).

remain irreversible, to $E_{p_a} = +0.55$ and $+0.81$ V (100 mV/s), and the appearance of a new weak irreversible reduction at $E_{p_c} = -1.10$ V, which is associated with the first oxidation (I_{p_a}-{+0.55 V}/I_{p_c}{−1.10 V} = 0.2 at 100 mV/s); the relative intensity of this reduction with respect to the parent oxidation does not increase significantly upon increasing the scan rate and decreases at scan rates below 50 mV/s. While we have been unable to characterize any oxidation products generated for **1**, we note that the analogous Co^{II} cubane $[Co_4(OMe)_4(L)_4(MeOH)_4]$ ($L^- =$ acac$^-$, dbm$^-$)[11] can be oxidized in the presence of acetate to the mixed-valence species $[Co_4(OMe)_4(L)_4(\mu\text{-}O_2CMe)_2]$;[23] it is therefore possible that addition of acetate to solutions of **1** may be stabilizing an oxidized $Ni^{II/III}_4$ cubane product, albeit not to such an extent as to make it isolable. Addition of a further 2 molar equiv of $Bu^n_4NO_2CMe$ to the above solution gives rise to broad irreversible voltammetric features only. Complex **3** under all the above conditions shows only broad, irreversible oxidative and reductive processes at high potentials ($E_{p_a} > +1.2$ V, $E_{p_c} < -2.0$ V) by cyclic voltammetry.

Description of Structures. ORTEP representations of **1** and **3** are shown in Figures 2 and 3, respectively; fractional coordinates and selected bond distances and angles for **1**·$2CH_2Cl_2$ and **3**·$2C_7H_8$ are listed in Tables 2 and 4 and Tables 3 and 5, respectively.

The solid-state structure of **1**·$2CH_2Cl_2$ contains discrete tetrameric molecules of formula $[Ni_4(OMe)_4(dbm)_4(MeOH)_4]$, each octahedral Ni^{II} ion being bound to three μ_3-OMe ligands, a chelating dbm^-, and one terminal MeOH ligand. The molecule lies on a general position within the unit cell and has virtual C_2 symmetry. Each MeOH hydroxyl group is intramolecularly hydrogen bonded to an O atom from a dbm^- ligand attached to a neighboring Ni ion, so that four of the six faces of the $[Ni_4(OMe)_4]^{4+}$ cubane core are spanned by hydrogen bonds (O···O_{av} = 2.716 Å); individual values and O−H···O angles are listed in Table 3. This has the effect of lowering the effective symmetry of the $[Ni_4(OMe)_4]^{4+}$ unit from T_d to D_{2d}, since the four faces spanned by hydrogen bonds exhibit shorter Ni···Ni distances and more acute Ni−O−Ni angles and Ni−O−O−Ni dihedral angles than the two not spanned in this fashion. For (Ni(1)−O(5)−O(7)−Ni(2), Ni(1)−O(5)−O(9)−Ni(4), Ni(2)−O(7)−O(11)−Ni(3), and Ni(3)−O(9)−O(11)−Ni(4): Ni···Ni = 3.046(2)−3.078(2) Å; Ni−O−Ni = 95.70(28)−97.27(26)°; Ni−O−O−Ni_{av} = 167.1°. For Ni(1)−O(7)−O(9)−Ni(3) and Ni(2)−O(5)−O(11)−Ni(4): Ni···Ni = 3.117(2) and 3.146(2) A; Ni−O−Ni = 98.93(27)−100.18(26); Ni−O−O−Ni_{av} = 174.2°). A similar pattern of intramolecular hydrogen bonding and structural distortions has also been observed in other alkoxide cubane complexes containing Ni^{II} and bound alcohol.[10,24] In the structurally related compounds $[Co_4(OMe)_4(acac)_4(MeOH)_4]$[11] and $[Fe_4(OMe)_4(dbm)_4(MeOH)_4]$,[25] however, this type of intramolecular hydrogen bonding causes the positioning of the Jahn−Teller axis of the high-spin Fe^{II} and Co^{II} ions along the (MeO)−M−(HOMe) (M = Fe, Co) vector, resulting in a lengthening of these M−(μ_3-O) bonds and thus in a cubane core of effective S_4 symmetry; differences in M−O−M angle between different faces of these latter cubane complexes are not pronounced. The Ni−O and intra-ligand distances and the bond angles around the octahedral Ni^{II} ions within **1** are unexceptional.

The structure of the bis(toluene) solvate of **3** contains well-separated $[Ni_4(N_3)_4(dbm)_4(EtOH)_4]$ cubane molecules, each azide ligand being symmetrically bound to three Ni^{II} ions in an end-on fashion. The disposition of ligands about the Ni^{II} ions and the effective molecular symmetry in **1** and **3** are identical; in particular, **3** shows patterns identical to those for **1** of intramolecular hydrogen bonding between ethanol hydroxyl groups and dbm^- O atoms (O···O_{av} = 2.703 Å; individual values are listed in Table 5) and of structural distortions within the $[Ni_4(N_3)_4]^{4+}$ core. (For (Ni(1)−N(5)−N(8)−Ni(2), Ni(1)−N(5)−N(14)−Ni(3), Ni(2)−N(8)−N(11)−Ni(4), and Ni(3)−

(23) (a) Bertrand, J. A.; Hightower, T. C. *Inorg. Chem.* **1973**, *12*, 206. (b) Dimitrou, K.; Christou, G. Unpublished result.

(24) (a) Bertrand, J. A.; Marabella, C.; Vanderveer, D. G. *Inorg. Chim. Acta* **1978**, *26*, 113. (b) Paap, F.; Bouwman, E.; Driessen, W. L.; de Graaf, R. A. G.; Reedijk, J. *J. Chem. Soc., Dalton Trans.* **1985**, 737.

(25) Taft, K. L.; Caneschi, A.; Pence, L. E.; Delfs, C. D.; Papaefthymiou, G. C.; Lippard, S. J. *J. Am. Chem. Soc.* **1993**, *115*, 11753.

Table 2. Selected Fractional Coordinates ($\times 10^4$) and Equivalent Isotropic Thermal Parameters ($\times 10$)[a] for Complex **1**·2CH_2Cl_2

atom	*x*	*y*	*z*	B_{eq}, Å^2
Ni(1)	8428(1)	1975(1)	2838(1)	21
Ni(2)	6649(1)	1951(1)	3464(1)	21
Ni(3)	8238(1)	2725(1)	4846(1)	19
Ni(4)	6620(1)	3294(1)	2414(1)	19
O(5)	6780(5)	2290(3)	2130(5)	24
C(6)	6136(9)	2145(5)	1044(9)	30
O(7)	8283(5)	1792(3)	4251(5)	21
C(8)	9030(9)	1191(5)	4978(9)	30
O(9)	8249(5)	2928(3)	3364(5)	20
C(10)	8961(8)	3283(5)	3387(8)	24
O(11)	6613(5)	2929(3)	3816(5)	19
C(12)	5838(7)	3318(5)	4165(8)	22
O(13)	8436(6)	2382(3)	1414(5)	30
C(14)	8563(10)	2042(6)	511(10)	42
O(15)	6927(6)	958(3)	2929(6)	31
C(16)	7112(15)	360(8)	3555(14)	82
O(17)	7997(5)	2405(3)	6173(5)	27
C(18)	8796(9)	2136(6)	7284(9)	36
O(19)	6703(5)	4243(3)	3034(5)	23
C(20)	5816(9)	4842(5)	2765(9)	32
O(21)	10013(5)	1676(3)	3591(6)	27
C(22)	10616(8)	1132(5)	3491(8)	27
C(23)	10282(8)	637(5)	2804(9)	29
C(24)	9268(9)	604(5)	2258(8)	25
O(25)	8440(5)	1042(3)	2272(6)	28
O(38)	5038(5)	2115(3)	2688(5)	25
C(39)	4436(8)	2102(5)	3118(9)	26
C(40)	4795(8)	1935(5)	4284(8)	26
C(41)	5878(8)	1758(5)	5096(8)	23
O(42)	6695(5)	1675(3)	4931(5)	25
O(55)	9816(5)	2535(3)	5879(5)	23
C(56)	10236(8)	2906(5)	6627(8)	20
C(57)	9688(8)	3570(5)	6736(8)	22
C(58)	8635(8)	3953(5)	6029(8)	21
O(59)	7992(5)	3710(3)	5210(5)	22
O(72)	5014(5)	3691(3)	1531(5)	25
C(73)	4485(8)	3954(5)	525(9)	27
C(74)	4954(8)	3950(5)	−209(8)	23
C(75)	6024(7)	3710(5)	50(8)	21
O(76)	6793(5)	3503(3)	1048(5)	23

[a] $B_{eq} = {}^4/_3 \sum\sum B_{ij} a_i a_j$.

N(11)−N(14)−Ni(4): Ni···Ni = 3.146(1)−3.177(1) Å; Ni−N−Ni = 94.82(21)−97.69(22)°; Ni−N−N−Ni_{av} = 167.1°. For Ni(1)−N(8)−N(14)−Ni(4) and Ni(2)−N(5)−N(11)−Ni(3): Ni···Ni = 3.231(1) and 3.239(1) Å; Ni−N−Ni = 99.13(22)−100.37(23)°; Ni−N−N−Ni_{av} = 175.5°.) Interestingly, comparison of **1** and **3** shows that substitution of N_3^- for MeO^- at the vertices of the $[Ni_4X_4]^{4+}$ cube causes an expansion of the core, each Ni···Ni distance increasing by approximately 0.1 Å, without changing the angular dimensions within the cubane unit. The azide ligands in **3** are linear, showing N−N bond lengths indistinguishable from those of Ni^{II} complexes containing end-on *doubly* bridging azides,[26] and are each bound symmetrically to three Ni ions, no significant variations in Ni−N distances being apparent within the cubane unit.

Magnetic Susceptibility Studies. Variable-temperature magnetic susceptibility measurements were performed on powder samples of **1** and **3** between 320 and 5.00 K (Figures 4 and 5). For both complexes, the observed effective magnetic moment

(26) (a) Arriortua, M. I.; Cortés, A. R.; Lezama, L.; Rojo, T.; Solans, X.; Font-Bardia, M. *Inorg. Chim. Acta* **1990**, *174*, 263. (b) Escuer, A.; Vicente, R.; Ribas, J. *J. Magn. Magn. Mater.* **1992**, *110*, 181. (c) Cortés, R.; Ruis de Larramendi, J. I.; Lezama, L.; Rojo, T.; Urtiaga, K.; Arriortua, M. *J. Chem. Soc., Dalton Trans.* **1992**, 2723. (d) Ribas, J.; Monfort, M.; Costa, R.; Solans, X. *Inorg. Chem.* **1993**, *32*, 695. (e) Vicente, R.; Escuer, A.; Ribas, J.; el Fallah, M. S.; Solans, X.; Font-Bardia, M. *Ibid.* **1993**, *32*, 1920. (f) Ribas, J.; Monfort, M.; Diaz, C.; Bastos, C.; Solans, X. *Ibid.* **1994**, *33*, 484.

Table 3. Selected Bond Distances (Å) and Angles (deg) for Complex **1**·2CH_2Cl_2

(a) Bonds

Ni(1)···Ni(2)	3.068(2)	Ni(2)···Ni(3)	3.078(2)
Ni(1)···Ni(3)	3.117(2)	Ni(2)···Ni(4)	3.146(2)
Ni(1)···Ni(4)	3.046(2)	Ni(3)···Ni(4)	3.076(2)
Ni(1)−O(5)	2.053(6)	Ni(3)−O(7)	2.046(6)
Ni(1)−O(7)	2.055(6)	Ni(3)−O(9)	2.051(6)
Ni(1)−O(9)	2.043(6)	Ni(3)−O(11)	2.065(6)
Ni(1)−O(13)	2.121(7)	Ni(3)−O(17)	2.120(6)
Ni(1)−O(21)	1.972(7)	Ni(3)−O(55)	2.015(6)
Ni(1)−O(25)	2.038(7)	Ni(3)−O(59)	2.035(6)
Ni(2)−O(5)	2.048(6)	Ni(4)−O(5)	2.056(7)
Ni(2)−O(7)	2.059(6)	Ni(4)−O(9)	2.047(6)
Ni(1)−O(11)	2.046(7)	Ni(4)−O(11)	2.055(6)
Ni(2)−O(15)	2.124(7)	Ni(4)−O(19)	2.110(6)
Ni(2)−O(38)	2.029(6)	Ni(4)−O(72)	2.014(6)
Ni(2)−O(42)	2.034(7)	Ni(4)−O(76)	2.031(6)
O(15)···O(25)	2.758	O(19)···O(59)	2.730
O(13)···O(76)	2.671	O(17)···O(42)	2.704
O(15)−H(17)	1.41	O(19)−H(25)	1.05
O(13)−H(13)	1.22	O(17)−H(21)	1.15

(b) Angles

O(5)−Ni(1)−O(7)	82.59(25)	O(7)−Ni(3)−O(9)	80.76(24)
O(5)−Ni(1)−O(9)	83.18(25)	O(7)−Ni(3)−O(11)	82.07(25)
O(5)−Ni(1)−O(13)	92.52(27)	O(7)−Ni(3)−O(17)	90.25(25)
O(5)−Ni(1)−O(21)	177.18(27)	O(7)−Ni(3)−O(55)	98.80(26)
O(5)−Ni(1)−O(25)	90.90(27)	O(7)−Ni(3)−O(59)	171.25(27)
O(7)−Ni(1)−O(9)	80.76(24)	O(9)−Ni(3)−O(11)	82.09(24)
O(7)−Ni(1)−O(13)	167.92(27)	O(9)−Ni(3)−O(17)	168.00(27)
P(7)−Ni(1)−O(21)	94.69(26)	O(9)−Ni(3)−O(55)	98.96(25)
O(7)−Ni(1)−O(25)	97.12(26)	O(9)−Ni(3)−O(59)	94.05(25)
O(9)−Ni(1)−O(13)	87.71(25)	O(11)−Ni(3)−O(17)	88.85(25)
O(9)−Ni(1)−O(21)	95.65(26)	O(11)−Ni(3)−O(55)	178.72(25)
O(9)−Ni(1)−O(25)	173.92(28)	O(11)−Ni(3)−O(59)	90.27(25)
O(13)−Ni(1)−O(21)	90.0(3)	O(17)−Ni(3)−O(55)	90.21(26)
O(13)−Ni(1)−O(25)	93.99(26)	O(17)−Ni(3)−O(59)	93.84(25)
O(21)−Ni(1)−O(25)	90.20(27)	O(55)−Ni(3)−O(59)	88.93(26)
O(5)−Ni(2)−O(7)	82.61(25)	O(5)−Ni(4)−O(9)	83.03(25)
O(5)−Ni(2)−O(11)	79.88(25)	O(5)−Ni(4)−O(11)	79.50(25)
O(5)−Ni(2)−O(15)	88.41(25)	O(5)−Ni(4)−O(19)	168.38(26)
O(5)−Ni(2)−O(38)	97.24(26)	O(5)−Ni(4)−O(72)	99.49(27)
O(5)−Ni(2)−O(42)	171.5(3)	O(5)−Ni(4)−O(76)	92.76(26)
O(7)−Ni(2)−O(11)	82.20(24)	O(9)−Ni(4)−O(11)	82.43(24)
O(7)−Ni(2)−O(15)	89.25(27)	O(9)−Ni(4)−O(19)	87.59(25)
O(7)−Ni(2)−O(38)	179.55(27)	O(9)−Ni(4)−O(72)	177.11(27)
O(7)−Ni(2)−O(42)	90.40(25)	O(9)−Ni(4)−O(76)	91.61(25)
O(11)−Ni(2)−O(15)	166.27(26)	O(11)−Ni(4)−O(19)	92.51(25)
O(11)−Ni(2)−O(38)	97.35(25)	O(11)−Ni(4)−O(72)	96.58(25)
O(11)−Ni(2)−O(42)	94.38(25)	O(11)−Ni(4)−O(76)	170.72(26)
O(15)−Ni(2)−O(38)	91.17(28)	O(19)−Ni(4)−O(72)	89.74(26)
O(15)−Ni(2)−O(42)	96.42(26)	O(19)−Ni(4)−O(76)	94.35(25)
O(38)−Ni(2)−O(42)	89.71(26)	O(72)−Ni(4)−O(76)	89.71(26)
Ni(1)−O(5)−Ni(2)	96.84(27)	Ni(3)−O(9)−Ni(4)	97.27(26)
Ni(1)−O(5)−Ni(4)	95.70(28)	Ni(2)−O(11)−Ni(3)	96.94(25)
Ni(2)−O(5)−Ni(4)	100.11(28)	Ni(2)−O(11)−Ni(4)	100.18(26)
Ni(1)−O(7)−Ni(2)	98.93(27)	O(13)−H(13)−C(76)	165.08
Ni(1)−O(7)−Ni(3)	96.45(26)	Ni(3)−O(11)−Ni(4)	96.58(25)
Ni(2)−O(7)−Ni(3)	97.12(26)	O(15)−H(17)−O(25)	145.07
Ni(1)−O(9)−Ni(3)	99.16(27)	O(17)−H(21)−O(42)	154.88
Ni(1)−O(9)−Ni(4)	96.31(27)	O(19)−H(25)−O(54)	168.37

(μ_{eff}) rises to a maximum of 9.66 μ_B, before slightly decreasing below 6.00 K. This maximum value may be compared with the spin-only value of 8.94 μ_B calculated for a $S = 4$ ground state expected for four ferromagnetically-coupled high-spin Ni^{II} ions with $g = 2.00$; the actual g value for Ni^{II} is expected to be greater than 2.0, however. Compound **3** reaches this maximum μ_{eff} at a higher temperature (20 K) than does **1** (10 K), implying a stronger overall ferromagnetic interaction for **3**. The magnetic moment data for **1** and **3** were interpreted on the basis of two models. First, a totally symmetric model was employed that treated each pairwise Ni···Ni interaction as equivalent (T_d symmetry, eq 1). The Kambe vector coupling method allows

Table 4. Selected Fractional Coordinates ($\times 10^4$) and Equivalent Isotropic Thermal Parameters ($\times 10$)[a] for Complex **3**·2C_7H_8

atom	*x*	*y*	*z*	B_{eq}, Å^2
Ni(1)	8936(1)	2057.6(4)	7163.6(3)	14
Ni(2)	6703(1)	2142.3(4)	6772.1(4)	15
Ni(3)	7754(1)	906.9(4)	7009.6(4)	14
Ni(4)	7951(1)	1623.0(4)	5942.8(3)	14
N(5)	7674(4)	1721(2)	7401(2)	15
N(6)	7499(4)	1737(2)	7871(2)	18
N(7)	7329(4)	1747(3)	8311(2)	30
N(8)	7943(4)	2349(2)	6460(2)	17
N(9)	8034(4)	2830(3)	6262(2)	20
N(10)	8118(5)	3270(3)	6077(3)	34
N(11)	6847(4)	1338(2)	6370(2)	14
N(12)	6161(4)	1094(2)	6087(2)	18
N(13)	5536(4)	869(3)	5825(3)	31
N(14)	8847(4)	1319(2)	6666(2)	14
N(15)	9552(4)	1034(2)	6630(2)	18
N(16)	10212(4)	764(3)	6603(3)	28
O(17)	9816(3)	1602(2)	7796(2)	19
C(18)	9993(6)	1801(4)	8354(3)	44
C(19)	10835(6)	1573(4)	8703(3)	34
O(20)	6939(3)	2883(2)	7263(2)	20
C(21)	6501(9)	3357(7)	7232(9)	173
C(22)	5653(6)	3560(4)	7242(4)	43
O(23)	7797(3)	219(2)	6475(2)	17
C(24)	8255(5)	−322(3)	6638(3)	21
C(25)	8683(5)	−588(3)	6181(3)	27
O(26)	6878(3)	2002(2)	5376(2)	22
C(27)	6794(6)	2114(4)	4799(3)	41
C(28)	5865(6)	2013(4)	4469(3)	43
O(29)	10020(3)	2376(2)	6876(2)	17
C(30)	10469(5)	2824(3)	7044(3)	15
C(31)	10275(5)	3174(3)	7483(3)	18
C(32)	9484(5)	3140(3)	7732(3)	16
O(33)	8823(3)	2756(2)	7612(2)	17
O(46)	5933(3)	2503(2)	6105(2)	18
C(47)	5016(5)	2529(3)	5999(3)	17
C(48)	4420(5)	2315(3)	6341(3)	21
C(49)	4701(5)	2021(3)	6854(3)	18
O(50)	5555(3)	1924(2)	7070(2)	21
O(63)	6763(3)	543(2)	7356(2)	17
C(64)	6883(5)	215(3)	7779(3)	15
C(65)	7796(5)	68(3)	8092(3)	18
C(66)	8664(5)	277(3)	7999(3)	16
O(67)	8774(3)	627(2)	7609(2)	18
O(80)	8949(3)	1918(2)	5552(2)	17
C(81)	9180(5)	1680(3)	5120(3)	17
C(82)	8905(5)	1135(3)	4926(3)	17
C(83)	8313(5)	756(3)	5136(3)	16
O(84)	7929(3)	863(2)	5565(2)	17

[a] $B_{eq} = {}^4/_3\sum\sum B_{ij}a_ia_j$.

$$\hat{H} = -2J(S_1{\cdot}S_2 + S_1{\cdot}S_3 + S_1{\cdot}S_4 + S_2{\cdot}S_3 + S_2{\cdot}S_4 + S_3{\cdot}S_4) \quad (1)$$

an expression to be derived for the energies by coupling the four Ni^{II} spins into a total spin $S_T = S_1 + S_2 + S_3 + S_4$.[27] By operator replacement, this then allows the spin Hamiltonian (eq 1) to be expressed in terms of S_T^2 only, so that the energies of the possible spin states (S_T) are given by eq 2. There are 19

$$E(S_T) = -J[S_T(S_T + 1)] \quad (2)$$

different spin states involving S_T values of 4, 3, 2, 1, and 0 with degeneracies of 1, 3, 6, 6, and 3, respectively. Substitution of these energies and degeneracies into the Van Vleck equation gives a theoretical expression for the molar susceptibility of these complexes *vs* temperature. Alternatively, a lower symmetry model was also examined to take into account the reduced symmetry of the cubane cores observed in the X-ray structures

(27) Kambe, K. *J. Phys. Soc. Jpn.* **1950**, *5*, 48.

Table 5. Selected Bond Distances (Å) and Angles (deg) for Complex **3**·C_7H_8

(a) Bonds

Ni(1)···Ni(2)	3.168(1)	Ni(3)−O(63)	1.970(4)
Ni(1)···Ni(3)	3.146(1)	Ni(3)−O(67)	1.983(4)
Ni(1)···Ni(4)	3.231(1)	Ni(3)−N(5)	2.132(6)
Ni(2)···Ni(3)	3.239(1)	Ni(3)−N(11)	2.100(5)
Ni(2)···Ni(4)	3.177(1)	Ni(3)−N(14)	2.132(5)
Ni(3)···Ni(4)	3.156(1)	Ni(4)−O(26)	2.070(4)
Ni(1)−O(17)	2.097(4)	Ni(4)−O(80)	1.981(4)
Ni(1)−O(29)	1.961(4)	Ni(4)−O(84)	1.990(5)
Ni(1)−O(33)	1.983(4)	Ni(4)−N(8)	2.109(6)
Ni(1)−N(5)	2.141(5)	Ni(4)−N(11)	2.150(5)
Ni(1)−N(8)	2.136(6)	Ni(4)−N(14)	2.113(6)
Ni(1)−N(14)	2.094(5)	N(5)−N(6)	1.225(7)
Ni(2)−O(20)	2.090(5)	N(6)−N(7)	1.150(7)
Ni(2)−O(46)	1.984(4)	N(8)−N(9)	1.233(7)
Ni(2)−O(50)	1.981(5)	N(9)−N(10)	1.134(8)
Ni(2)−N(5)	2.117(5)	N(11)−N(12)	1.232(7)
Ni(2)−N(8)	2.111(5)	N(12)−N(13)	1.129(7)
Ni(2)−N(11)	2.138(6)	N(14)−N(15)	1.222(7)
Ni(3)−O(23)	2.076(4)	N(15)−N(16)	1.145(7)
O(17)···O(67)	2.702(8)	O(23)···O(84)	2.723(8)
O(20)···O(33)	2.690(8)	O(26)···O(46)	2.695(8)

(b) Angles

O(17)−Ni(1)−O(29)	92.85(18)	N(11)−Ni(3)−N(14)	83.54(20)
O(17)−Ni(1)−O(33)	95.72(18)	O(26)−Ni(4)−O(80)	92.18(18)
O(17)−Ni(1)−N(5)	92.07(19)	O(26)−Ni(4)−O(84)	96.67(19)
O(17)−Ni(1)−N(8)	168.15(20)	O(26)−Ni(4)−N(8)	88.92(20)
O(17)−Ni(1)−N(14)	89.06(20)	O(26)−Ni(4)−N(11)	86.49(19)
O(29)−Ni(1)−O(33)	92.42(18)	O(26)−Ni(4)−N(14)	165.61(19)
O(29)−Ni(1)−N(5)	174.57(19)	O(80)−Ni(4)−O(84)	91.80(19)
O(29)−Ni(1)−N(8)	92.42(20)	O(80)−Ni(4)−N(8)	95.65(20)
O(29)−Ni(1)−N(14)	93.79(19)	O(80)−Ni(4)−N(11)	177.65(20)
O(33)−Ni(1)−N(5)	89.38(20)	O(80)−Ni(4)−N(14)	98.18(19)
O(33)−Ni(1)−N(8)	94.66(20)	O(84)−Ni(4)−N(8)	170.51(20)
O(33)−Ni(1)−N(14)	171.97(20)	O(84)−Ni(4)−N(11)	90.28(20)
N(5)−Ni(1)−N(8)	82.32(20)	O(84)−Ni(4)−N(14)	92.96(20)
N(5)−Ni(1)−N(14)	83.99(20)	N(8)−Ni(4)−N(11)	82.40(21)
N(8)−Ni(1)−N(14)	80.00(21)	N(8)−Ni(4)−N(14)	80.19(21)
O(20)−Ni(2)−O(46)	97.78(19)	N(11)−Ni(4)−N(14)	82.80(20)
O(20)−Ni(2)−O(50)	93.16(19)	Ni(1)−N(5)−Ni(2)	96.14(21)
O(20)−Ni(2)−N(5)	86.79(20)	Ni(1)−N(5)−Ni(3)	94.82(21)
O(20)−Ni(2)−N(8)	87.97(19)	Ni(1)−N(5)−N(6)	124.9(4)
O(20)−Ni(2)−N(11)	164.66(19)	Ni(2)−N(5)−Ni(3)	99.35(22)
O(46)−Ni(2)−O(50)	92.28(19)	Ni(2)−N(5)−N(6)	116.9(4)
O(46)−Ni(2)−N(5)	171.02(19)	Ni(3)−N(5)−N(6)	119.2(5)
O(46)−Ni(2)−N(8)	88.93(20)	N(5)−N(6)−N(7)	179.3(7)
O(46)−Ni(2)−N(11)	94.17(20)	Ni(1)−N(8)−Ni(2)	96.49(23)
O(50)−Ni(2)−N(5)	95.20(20)	Ni(1)−N(8)−Ni(4)	99.13(22)
O(50)−Ni(2)−N(8)	178.22(21)	Ni(1)−N(8)−N(9)	120.1(4)
O(50)−Ni(2)−N(11)	95.96(20)	Ni(2)−N(8)−Ni(4)	97.69(22)
N(5)−Ni(2)−N(8)	83.48(20)	Ni(2)−N(8)−N(9)	120.2(4)
N(5)−Ni(2)−N(11)	80.13(20)	Ni(4)−N(8)−N(9)	118.3(5)
N(8)−Ni(2)−N(11)	82.65(20)	N(8)−N(9)−N(10)	179.4(7)
O(23)−Ni(3)−O(63)	92.85(18)	Ni(2)−N(11)−Ni(3)	99.71(23)
O(23)−Ni(3)−O(67)	96.61(18)	Ni(2)−N(11)−Ni(4)	95.64(22)
O(23)−Ni(3)−N(5)	167.70(19)	Ni(2)−N(11)−N(12)	121.8(4)
O(23)−Ni(3)−N(11)	88.79(20)	Ni(3)−N(11)−Ni(4)	95.92(21)
O(23)−Ni(3)−N(14)	89.25(19)	Ni(3)−N(11)−N(12)	121.4(4)
O(63)−Ni(3)−O(67)	91.63(18)	Ni(4)−N(11)−N(12)	116.6(4)
O(63)−Ni(3)−N(5)	94.82(19)	N(11)−N(12)−N(13)	179.4(7)
O(63)−Ni(3)−N(11)	97.63(19)	Ni(1)−N(14)−Ni(3)	96.20(21)
O(63)−Ni(3)−N(14)	177.61(20)	Ni(1)−N(14)−Ni(4)	100.37(23)
O(67)−Ni(3)−N(5)	92.77(19)	Ni(1)−N(14)−N(15)	121.5(4)
O(67)−Ni(3)−N(11)	169.04(20)	Ni(3)−N(14)−Ni(4)	96.07(21)
O(67)−Ni(3)−N(14)	87.00(19)	Ni(3)−N(14)−N(15)	117.4(4)
N(5)−Ni(3)−N(11)	80.68(20)	Ni(4)−N(14)−N(15)	120.0(4)
N(5)−Ni(3)−N(14)	83.30(20)	N(14)−N(15)−N(16)	179.0(7)

of **1** and **3** (D_{2d}, eq 3), where J_1 corresponds to the interaction

$$H = -2J_1(S_1{\cdot}S_2 + S_3{\cdot}S_4) - 2J_2(S_1{\cdot}S_3 + S_1{\cdot}S_4 + S_2S_3 + S_2{\cdot}S_4) \quad (3)$$

across faces of the cubane not spanned by hydrogen bonds and

Table 6. Literature Structural (Å, deg) and Magnetochemical (cm^{-1}) Data for $[Ni_4(\mu_3\text{-}OR)_4]^{4+}$ Cubane Complexes

complex[b]	Ni−(μ-O)$_{av}$	Ni···Ni	Ni−O−Ni$_{av}$	Ni−O−O−Ni$_{av}$	J	g	ref
$[Ni_4(\mu_3\text{-}OMe)_4(sal)_4(EtOH)_4]$	2.039	3.081	97.73	169.3	7.46	2.15	10
$[Ni_4(\mu_3\text{-}OH)_4(chta)_4(NO_3)_4]$	2.088	3.176	99.0	167.7	−0.57	2.20	12
$[Ni_4(\mu_3\text{-}OMe)_4(TMB)_4(\mu\text{-}O_2CMe)_2]^{2+}$	2.067[a]	2.998[a]	93.0[a]	156.2[a]	17.5[a]	2.00	13
	2.070	3.193	100.9	174.3	−9.1		
$[Ni_4(\mu_3\text{-}OH)_4(tzdt)_4(py)_4]$	2.06	3.06	95.85	162.5	17.5	2.0	14
	2.07	3.20	103.2	179.6	−22		
$[Ni_4(\mu_3\text{-}OMe)_4(dbm)_4(MeOH)_4]$	2.050	3.067	96.7	167.1	12.2	2.05	this work
	2.053	3.132	99.6	174.2	−3.4		

[a] This face of this cubane is bridged by an η^2,μ-acetate group, in addition to the two μ-OMe ligands. This data point was therefore omitted from the solid line correlations in Figure 6. [b] chta = *r*-1-*c*-3-*c*-5-triaminocyclohexane; dbmH = dibenzoylmethane; py = pyridine; salH = salicylaldehyde; TMB = 2,5-dimethyl-2,5-diisocyanohexane; tzdtH = 1,3-thiazolidine-2-thione.

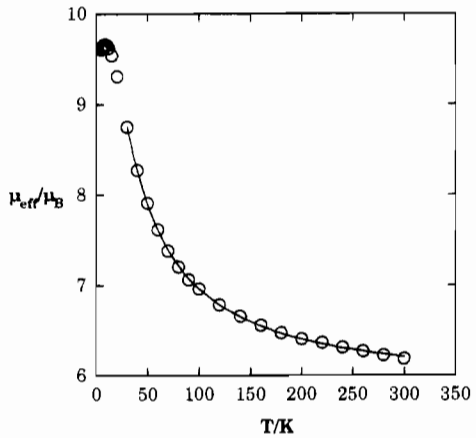

Figure 4. Plot of μ_{eff} versus T for $[Ni_4(OMe)_4(dbm)_4(MeOH)_4]$ (**1**). The solid line represents the fit to a two-J model; see the text for the fitting parameters.

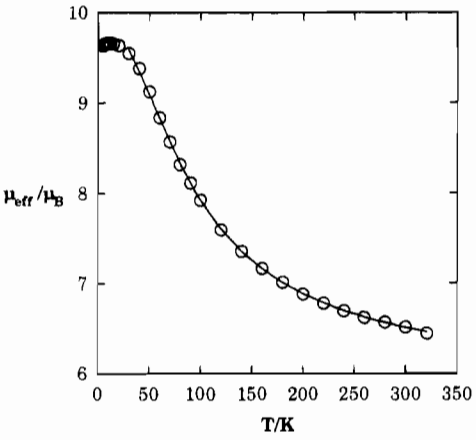

Figure 5. Plot of μ_{eff} versus T for $[Ni_4(N_3)_4(dbm)_4(EtOH)_4]$ (**3**). The solid line represents the fit to a one-J model; see the text for fitting parameters.

J_2 to the interaction across faces of the cubane that are spanned in this manner. The definition of the quantities $S_A = S_1 + S_2$, $S_B = S_3 + S_4$, and $S_T = S_A + S_B$ allows the spin Hamiltonian of eq 3 to be written in an equivalent operator form and leads to an expression for the spin state (S_T) energies (eq 4), which

$$E(S_T,S_A,S_B) = -J_1[S_A(S_A + 1) + S_B(S_B + 1)] - J_2[S_T(S_T + 1) - S_A(S_A + 1) - S_B(S_B + 1)] \quad (4)$$

are substituted into the Van Vleck equation as before. There are 19 spin states involving S_A, S_B = 2, 1, 0 and S_T varying from $|S_A + S_B|$ to $|S_A - S_B|$ in integer increments. In addition, for **1** and **3**, a satisfactory fit of the experimental data obtained at temperatures below 70 K using both models was only obtained when a Weiss constant (Θ) was introduced to account for intermolecular interactions in the solid state, by substitution of the term $(T - \Theta)$ for the temperature parameter T in the pre-exponential factor of the Van Vleck equation;[28] this follows the approach of Bertrand *et al.*, who also modeled intermolecular effects in the variable-temperature magnetic susceptibility behavior of the closely related complex $[Ni_4(OMe)_4(acac)_4(MeOH)_4]$ in this way.[11] For both compounds, satisfactory fits of data obtained at temperatures ≥30 K were now obtained (*vide infra*), with g and J values similar to those obtained for higher temperature fits. If data from temperatures below 30 K were also included, satisfactory fits were not possible using these equations, however, presumably owing to effects such as zero-field splitting within the $S = 4$ ground state spin manifold. Therefore, we employed data only for $T \geq 30$ K in data fitting for both complexes.

The effective magnetic moment data for **1** at temperatures ≥30 K were better fit by the two-J (D_{2d}) equation, the fitting parameters being $J_1 = -3.4$ cm^{-1}, $J_2 = +12.2$ cm^{-1}, $g = 2.05$, and $\Theta = +2.1$ K (Figure 4). Utilization of the one-J (T_d) model for this complex afforded $J = +5.9$ cm^{-1}, $g = 2.08$, and $\Theta = -0.03$ K, this J value being indistinguishable from that previously reported for $[Ni_4(OMe)_4(acac)_4(MeOH)_4]$ ($J = +5$ cm^{-1}).[11] However, the fits obtained from the one-J model were noticeably inferior to those obtained from the two-J equation. The similarity of the two-J g value and Weiss constant for **1** to those obtained for **3** (*vide infra*) and the good agreement shown by the two-J model with the J *vs* Ni−O−Ni angle correlation described below (Table 6, Figure 6), also support this interpretation.

The observation of two discrete J values for **1** is consistent with the two types of $[Ni_2(OMe)_2]$ faces present in this cluster. The dependence of J on the Ni−(μ-O)−Ni angle has previously been noted for other $[Ni_4(OR)_4]^{4+}$ cubanes,[12-14] and the magnetic properties of some have also necessitated a two-J interpretation.[13,14] It is noteworthy that J might also depend on other structural parameters, in particular the Ni−(μ-O) distances and Ni−O−O−Ni dihedral angles. We have plotted the observed J values for **1** and other structurally-characterized $[Ni_4(OR)_4]^{4+}$ cubanes against average Ni−O−Ni angles and Ni−O−O−Ni dihedral angles in these complexes,[10,12-14] taking into account those cases where the magnetic data were consistent with a two-J interpretation[13,14] (Table 6 and Figure 6). For both these plots, a fairly linear correlation between J and the relevant structural parameter is observed (dashed lines); these correlations are much improved (solid lines), however, when one interaction involving an additional bridging acetate ligand ($J = +17.5$ cm^{-1}, Ni−O−Ni = 93.0°, Ni−O−O−Ni = 156.2°), which should provide an additional pathway for antiferromagnetic coupling, in the complex $[Ni_4(OMe)_4(O_2CMe)_2(tmb)_4]^{2+}$ (tmb = 2,5-dimethyl-2,5-isocyanohexane, Table 6)[13] is omitted from consideration. The remaining complexes, whose exchange inter-

(28) Ginsberg, A. P.; Lines, M. E. *Inorg. Chem.* **1972**, *11*, 2289.

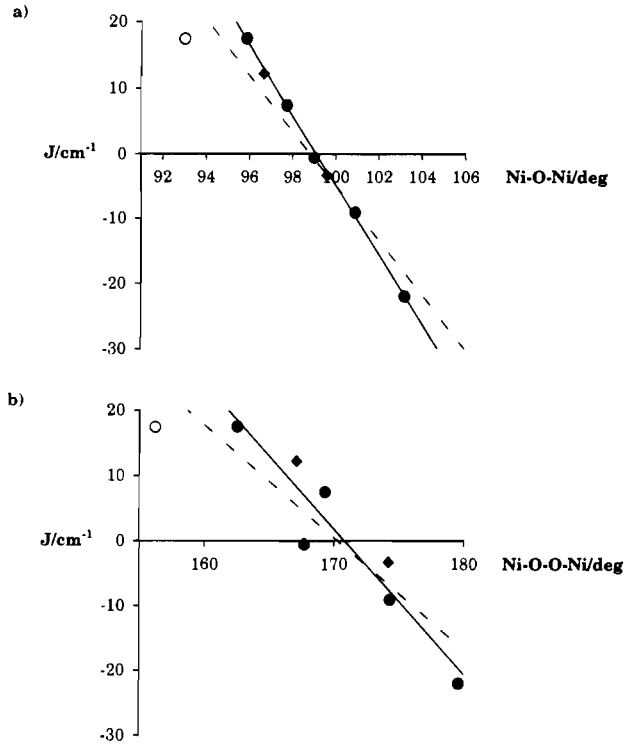

Figure 6. Effect of (a) average Ni−O−Ni angle and (b) average Ni−O−O−Ni torsion angle on J for $[Ni_4(OR)_4]^{4+}$ cubanes: (●) literature data (refs 10, 12, 13, 14); (◆) this work. Dashed lines represent lines of best fit for all data; solid lines, for data omitting one interaction (○) involving an additional acetate bridge (ref 13; see text, Table 6).

actions are mediated *only* by RO^- (R = H, Me) bridges, now show an excellent correlation between J and Ni−O−Ni angle. This is the first such correlation to be reported for magnetic interactions transmitted through symmetric, triply-bridging ligands. Structurally, it is impossible to separate the effects of the Ni−O−Ni and Ni−O−O−Ni parameters; however, a theoretical study of the effect of decreasing Cu−O−O−Cu dihedral angle on the singlet−triplet gap in bent $[Cu_2(OH)_2]^{2+}$ dimers published by Kahn and co-workers[29] suggests that the range of average dihedral angles observed in the $[Ni_4(OR)_4]^{4+}$ cubanes (156.2 < Ni−O−O−Ni < 179.6°) should not cause a variation in J of more than approximately 20% for a constant Ni−O−Ni angle. In addition, a related study on $[Cu_4(OR)_4]^{4+}$ cubanes (*vide infra*) suggested that for these complexes J was not affected by bending of the Cu_2O_2 planes.[30] Hence, we believe the major contributor to the superexchange constants observed in $[Ni_4(OR)_4]^{4+}$ cubanes to be the Ni−O−Ni angle. While ranges of average bond lengths Ni−$(\mu$-O$)_{av}$ = 2.04−2.09 Å and Ni···Ni$_{av}$ = 3.00−3.20 Å are observed in these complexes, there is no obvious trend relating these distances and $|J|$, implying that this magnitude of variation in Ni−$(\mu$-O) and Ni···Ni distances has only a small effect on the observed J values by comparison with the above angle parameters.

Since the original report by Hatfield and Hodgson of a linear relationship between $2J$ and the Cu−$(\mu$-O)−Cu angle in complexes containing a planar $[Cu_2(\mu\text{-}OH)_2]^{2+}$ bridge,[31] other

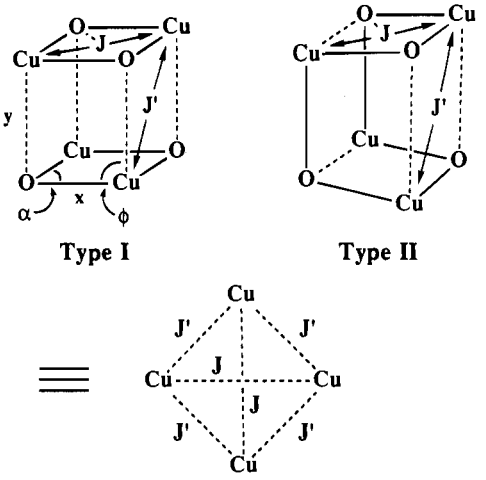

Figure 7. Structures of $[Cu_4(OR)_4]^{4+}$ cubane complexes: (a) "dimer of dimers" (type I); (b) "trans-annulated ring" (type II).

correlations relating J to a structural parameter have been reported for complexes containing the following core motifs: (i) J *vs* M−X−M bridging angle; planar $[Cu_2(\mu\text{-}X)_2]^{2+}$ (X^- = halide ion),[32] $[Cu_2(\mu\text{-}OR)_2]^{2+}$ (R = alkyl),[30] $[Cr_2O_2]^{2+}$,[33] and $[Ni_2(\mu\text{-}OR)_2]^{2+}$ (R = aryl);[34] (ii) J *vs* M−X−X−M dihedral or torsion angle; bent $[Cu_2(\mu\text{-}OH)_2]^{2+}$ [29] and $[Ni_2(\mu\text{-}1,3\text{-}N_3)_x]^{2+}$ (x = 1,2);[35] and (iii) J *vs* M−X distance; $[Fe^{III}_2(\mu\text{-}O)(\mu\text{-}Y)_x]^{n+}$ (Y^- = RO^-, $R'CO_2^-$; R = H, alkyl, aryl; R′ = alkyl, aryl; x = 0−2).[36] In addition, the magnetic and structural properties of a large number of $[Cu_4(\mu_3\text{-}OR)_4]^{4+}$ (R = H, alkyl) "cubanes" have been described,[30,37-42] these latter compounds being of particular relevance to this study. Structurally, these complexes are best regarded as dimers of dimers (effective C_{2v} symmetry; Figure 7, "type I") or trans-annulated rings (effective S_4 symmetry, "type II"), with intra-dimer and intra-ring Cu−O distances x varying from 1.9 to 2.2 Å and inter-dimer or trans-annular Cu−O distances y varying from 2.2 to 3.0 Å between compounds. A systematic study of a series of $[Cu_4(OR)_4]^{4+}$ (R = alkyl) complexes by Haase and co-workers[30] concluded that magnetochemically both type I and type II compounds are best described as dimers of dimers (Figure 7), that the

(29) (a) Charlot, M. F.; Jeannin, S.; Jeannin, Y.; Kahn, O.; Lucrece-Abaul, J.; Martin-Frere, J. *Inorg. Chem.* **1979**, *18*, 1675. (b) Charlot, M. F.; Kahn, O.; Jeannin, S.; Jeannin, Y. *Ibid.* **1980**, *19*, 1410.
(30) (a) Merz, L.; Haase, W. *J. Chem. Soc., Dalton Trans.* **1978**, 1595. (b) Merz, L.; Haase, W. *Ibid.* **1980**, 875. (c) Mergehenn, R.; Merz, L.; Haase, W. *Ibid.* **1980**, 1703. (d) Laurent, J.-P.; Bonnet, J.-J.; Nepveu, F.; Astheimer, H.; Walz, L.; Haase, W. *Ibid.* **1982**, 2433. (e) Schwabe, L.; Haase, W. *Ibid.* **1985**, 1909.
(31) Crawford, V. H.; Richardson, H. W.; Wasson, J. R.; Hodgson, D. J.; Hatfield, W. H. *Inorg. Chem.* **1976**, *15*, 2107.
(32) (a) Roundhill, S. G. N.; Roundhill, D. M.; Bloomquist, D. R.; Landee, C.; Willett, R. D.; Dooley, D. M.; Gray, H. B. *Inorg. Chem.* **1979**, *18*, 831. (b) Livermore, J. C.; Willett, R. D.; Gaura, R. M.; Landee, C. P. *Ibid.* **1982**, *21*, 1403. (c) Fletcher, R.; Hansen, J. J.; Livermore, J.; Willett, R. D. *Ibid.* **1983**, *22*, 330.
(33) Charlot, M. F.; Kahn, O.; Drillon, M. *Chem. Phys.* **1982**, *70*, 177.
(34) Nanda, K. K.; Thompson, L. K.; Bridson, J. N.; Nag, K. *J. Chem. Soc., Chem. Commun.* **1994**, 1337.
(35) (a) Ribas, J.; Monfort, M.; Diaz, C.; Bastos, C.; Solans, X. *Inorg. Chem.* **1993**, *32*, 3557. (b) Escuer, A.; Vicente, R.; Ribas, J.; El Fallah, M. S.; Solans, X.; Font-Bardía, M. *Ibid.* **1993**, *32*, 3727.
(36) Gorun, S. M.; Lippard, S. J. *Inorg. Chem.* **1991**, *30*, 1625.
(37) (a) Haase, W. *Chem. Ber.* **1973**, *106*, 3132. (b) Mergehenn, R.; Haase, W. *Acta Crystallogr.* **1977**, *B33*, 1877. (c) Megehenn, R.; Haase, W. *Ibid.* **1977**, *B33*, 2734.
(38) (a) Estes, E. D.; Hodgson, D. J. *Inorg. Chem.* **1975**, *14*, 334. (b) Hall, J. W.; Estes, W. E.; Estes, E. D.; Scaringe, R. P.; Hatfield, W. E. *Inorg. Chem.* **1977**, *16*, 1572.
(39) Nepveu, F. *Inorg. Chim. Acta* **1987**, *134*, 43.
(40) (a) Nieminen, K. *Acta Chem. Scand., Ser. A* **1977**, *31*, 693. (b) Nieminen, K. *Ibid.* **1979**, *33*, 375. (c) Muhonen, H. *Ibid.* **1980**, *34*, 79. (d) Ahlgrén, M.; Hämäläinen, R.; Turpeinen, U.; Smolander, K. *Acta Crystallogr.* **1979**, *B35*, 2870. (e) Turpeinen, U.; Hämäläinen, R.; Ahlgrén, M. *Ibid.* **1980**, *B36*, 927. (f) Ahlgrén, M.; Turpeinen, U.; Hämäläinen, R. *Ibid.* **1982**, *B38*, 429.
(41) (a) Matsumoto, N.; Tsutsumi, T.; Ohyoshi, A.; Okawa, H. *Bull. Chem. Soc., Jpn.* **1983**, *56*, 1388. (b) Jezowska-Trzebiatowska, B.; Olejnik, Z.; Lis, T. *J. Chem. Soc., Dalton Trans.* **1981**, 251. (c) Walz, L.; Paulus, H.; Haase, W.; Langhof, H.; Nepveu, F. *Ibid.* **1983**, 657. (d) Astheimer, H.; Nepveu, F.; Walz, L.; Haase, W. *Ibid.* **1985**, 315.
(42) Sletten, J.; Sørensen, A.; Julve, M.; Journaux, Y. *Inorg. Chem.* **1990**, *29*, 5054.

Table 7. Literature Structural (Å, deg) and Magnetochemical (cm^{-1}) Data for Dinuclear and Polymeric Complexes of Octahedral Ni^{II}-Containing Planar $[Ni_2(\eta^1,\mu\text{-}N_3)_2]^{2+}$ Bridges

complex[a]	Ni−(μ-N)av	Ni···Ni	Ni−N−Ni$_{av}$	N−N−Ni−Ni$_{av}$	J	g	ref
$[Ni_2(\mu\text{-}N_3)_4(en)_2]_x$[a]	2.121	3.241	101.3	139.5−154.1	14.8	2.27	26f
$[Ni_2(\mu\text{-}N_3)_4(tn)_2]_x$[a]	2.106	3.310	103.7	146.0−165.7	17.6	2.54	26f
$[Ni_2(\mu\text{-}N_3)_2(N_3)_2(terpy)_2]$	2.118	3.276	101.3	140.4	20.1	2.26	26a
$[Ni_2(\mu\text{-}N_3)_2(en)_4]^{2+}$	2.134	3.369	104.3	173.3	20.9	2.31	26f
$[Ni_2(\mu\text{-}N_3)_2(2,3,2\text{-}N_4)_2]^{2+}$	2.167	3.423	104.9	174.6	33.8	2.27	26e
$[Ni_2(\mu\text{-}N_3)_2(N_3)_2(pepci)_2]$	2.127	3.297	101.6	157.6	36.3	2.11	26c
$[Ni_2(\mu\text{-}N_3)_2(N_3)_2(Medpt)_2]$[b]	2.193	3.448	103.7	*c*	45.6	2.21	26b
	2.202	3.470	104.0	*c*	75.7	2.23	26b

[a] Complexes are polymers containing three crystallographically unique $Ni_3(N)_2$ bridges per asymmetric unit, whose magnetic properties were interpreted in terms of a single J value. The structural parameters quoted are average values for the entire structure. [b] Complex shows a magnetic transition at 150−120 K. Parameters given are for the low- and high-temperature forms, respectively. [c] Not reported. [d] The complexes are ranked in order of increasing J. en = 1,2-diaminoethane; Medpt = 3,3′-diamino-*N*-methyldipropylamine; pepci = *N*′-(2-pyridin-2-ylethyl)pyridine-2-carbaldimine; terpy = 2,2′,6′,2″-terpyridine; tn = 1,3=diaminopropane; 2,3,2-N4 = *N*,*N*′-bis(2-aminoethyl)-1,3-diaminopropane.

(antiferromagnetic) intra-dimer exchange interaction J follows a Hatfield and Hodgson-type correlation with Cu−O−Cu angle (α) for a constant Cu−O distance (x),[30b] but that the (weakly ferromagnetic) inter-dimer interaction J' depends only on the Cu···O distance (y)[30b,d] or the angle between the two dimeric Cu_2O_2 planes,[30a] no effect of the Cu···O−Cu angle (ϕ) on J' being evident.[30a,b] This contrasts with the results of this study, where the $[Ni_4(OR)_4]^{4+}$ compounds are best regarded as genuine cubane structures with no lengthened Ni···O distances, and all interactions within the $[Ni_4(OR)_4]^{4+}$ cubanes follow a Hatfield and Hodgson-type correlation. These differences are readily rationalized by considering the electronic configurations at the two metal ions. The Jahn−Teller elongations expected for d^9 Cu^{II} ions cause the marked distortions within the $[Cu_4(OR)_4]^{4+}$ structures, while the absence of an unpaired electron in the d_{z^2} orbital perpendicular to the intra-dimer planes leads to very weak exchange interactions in this direction. The high-spin d^8 Ni^{II} configuration is not Jahn−Teller active, however, and has σ-symmetry magnetic orbitals ($d_{x^2-y^2}$ and d_{z^2}) aligned along all three geometric axes, resulting in (geometric factors notwithstanding) more isotropic magnetic interactions within the cubane core.

In contrast to the behavior observed for **1**, the μ_{eff} data for **3** at temperatures ≥30 K were well reproduced by the one-J model (Figure 5), giving $J = +11.9$ cm^{-1}, $g = 2.05$, and $\Theta = +3.0$ K. In this case, utilization of the two-J model did not result in improved fits or in significant splitting (<0.1 cm^{-1}) of the J_1 and J_2 parameters. The observation of a ferromagnetic interaction within this complex is consistent with both the previously proposed accidental orthogonality[16] and spin polarization[17] rationalizations for the sign of magnetic exchange interactions transmitted through azide bridges. The observed J value is also the smallest yet reported for coupling between Ni^{II} ions mediated by end-on azide bridges, however (Table 7),[26] consistent with the presence of μ_3-N_3^-, as opposed to μ_2-N_3^-, ligands in **3**. The lack of dependence of J on the varying Ni−N−Ni angles within the cubane core is striking, however, and contrasts with the behavior of **1**. This result is interesting in the light of a recent study of dinuclear Cu^{II}_2 complexes containing both η^1,μ-azide and 1,2-diazine bridges,[15] which showed a similar pattern of variation of $2J$ with Cu−N(azide)−Cu angle as did analogous $[Cu^{II}_2(\mu\text{-OH})(\mu\text{-1,2-diazine})]$ complexes with Cu−O−Cu angle, leading to the suggestion that $[Cu_2(\eta^1,\mu\text{-}N_3)_x]^{(4-x)+}$ (x = 1, 2) complexes should also follow a Hatfield and Hodgson-type J *vs* Cu−N−Cu linear correlation. Clearly, this is not the case for **3**.

In order to examine the possibility of a correlation between J and Ni−N−Ni bridging angle in doubly end-on azide bridged species, we have tabulated and plotted J *vs* average Ni−N−Ni angles for a series of known complexes of formula $[Ni_2(\eta^1,\mu\text{-}N_3)_2(L)(N_3)_x]^{(2-x)+}$ (L = N-donor chelate, x = 0, 2; Table 7, Figure 8a) containing octahedral Ni^{II} ions.[26] It is clear from this graph that there is no simple linear correlation relating J with Ni−N−Ni angle for these compounds. While a detailed analysis of the magnetic and structural properties of dinuclear Ni^{II} complexes is outside the scope of this work, we make the following observations. First, there appears to be a trend for J to become more ferromagnetic with increasing average Ni−(μ-N) distances, although a plot of Ni−(μ-N)$_{av}$ *vs* J is only moderately linear (Figure 8b). In this regard, the magnetostructural properties of the complex $[Ni_2(\mu\text{-}N_3)_2(N_3)_2(Medpt)_2]$ (Medpt = 3,3′-diamino-*N*-methyldipropylamine) are of interest.[26b] This complex shows a magnetic transition occurring between 150 and 120 K, resulting in a decrease in J from 75.7 cm^{-1} (high-temperature form) to 45.6 cm^{-1} (low-temperature form); a comparison of two single-crystal X-ray structures of this compound obtained at high and low temperatures showed differences only in Ni−N and Ni···Ni distances between the two

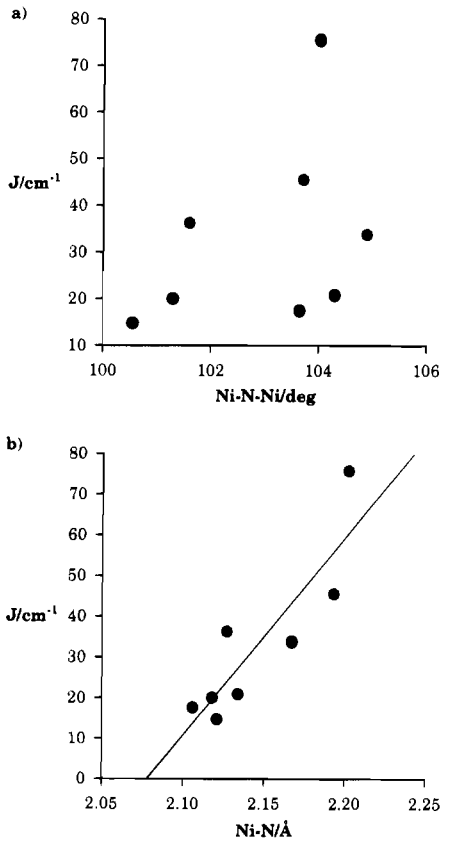

Figure 8. Effect of (a) the average Ni−N−Ni angle and (b) the average Ni−(μ-N) distance on J for dimeric and polymeric Ni^{II} complexes containing the planar $[Ni_2(\eta^1,\mu\text{-}N_3)_2]^{2+}$ bridging motif.

forms (Table 7), the two structures showing indistinguishable Ni−N−Ni bridge angles and crystal packing. Second, while the central Ni_2N_2 bridge in all these compounds is exactly or approximately planar, in no case are bridging azide ligands coplanar with the Ni_2N_2 bridging plane, a range of Ni−Ni−N−N dihedral angles being observed for these compounds (Table 7). Since it has been recently demonstrated that magnetochemical exchange between Ni^{II} ions mediated by end-to-end azide bridges is predominantly governed by the Ni−(N−N−N)−Ni torsion angle and M−(N−N−N)$_2$−M dihedral angle within the $[Ni_2(\mu\text{-}1,3\text{-}N_3)_x]^{2+}$ (x = 1 and 2, respectively) unit,[35] it is not unreasonable to suspect that the Ni−Ni−N−N torsion angle may also play a role in the magnetic properties of $[Ni_2(\eta^1,\mu\text{-}N_3)_2]^{2+}$ complexes. Either scenario would explain the behavior of **3**, since the Ni−(μ-N) distances (Table 5) and Ni−Ni−N−N torsions (Ni−Ni−N−N_{av} = 127.8−133.0°) in the structure of **3** are relatively invariant for all faces of the $[Ni_4(\eta^1,\mu_3\text{-}N_3)_4]^{4+}$ cubane core. In any case, it is noteworthy that the apparent lack of correlation of J with the Ni−(μ-N)−Ni angle in doubly end-on azide-bridged complexes contrasts with the previously described behavior of planar $[M_2(\mu\text{-}OR)_2]^{2+}$ (M = Cu, R = H, alkyl; M = Ni, R = aryl) complexes and is consistent with the difference in properties between **1** and **3**.

Finally, we note that the apparent non-dependence of J on the Ni−N−Ni bridge angles for **3** is one of a series of recent observations on the magnetic properties of polynuclear end-on azide-bridged complexes that emphasize the difficulty of achieving a complete rationalization of superexchange through azide ligands. We also count here the aforementioned properties of $[Ni_2(\mu\text{-}N_3)_2(N_3)_2(Medpt)_2]$[26b] and recent reports of previously unprecedented antiferromagnetic coupling mediated by end-on azide-bridging ligands both in Cu^{II}_2 complexes with unusually large Cu−N−Cu angles (Cu−N−Cu > 108.5°)[15] and in a $[Ni_2(\eta^1,\mu\text{-}N_3)_3]^+$ complex with unusually acute Ni−N−Ni angles averaging 84°.[43] By comparison, a theoretical study of the accidental orthogonality model in $[Cu_2(\eta^1,\mu\text{-}N_3)_2]^{2+}$ dimers predicted a switch from ferromagnetic to antiferromagnetic coupling only for Cu−(μ-N)−Cu angles above 103°.[16] By themselves, neither of the previously proposed accidental orthogonality[15,16] and spin polarization[17] models of superexchange transmitted through end-on bridging-azide ligands appears to be able to explain all of these observations, and it may be that a more intricate explanation of superexchange in end-on azide-bridged complexes incorporating both these effects is necessary.

Acknowledgment. This work was supported by NSF Grant 9311904. We thank M. W. Wemple (Indiana University) for the ^{2}H NMR spectra and for helpful discussions.

Supporting Information Available: Textual presentations of the structure solutions and complete tables of crystallographic data, fractional coordinates, anisotropic thermal parameters, bond lengths and angles, and molar magnetic susceptibility *vs* temperature data for **1** and **3** (46 pages). Ordering information is given on any current masthead page.

IC950292I

(43) Ribas, J.; Monfort, M.; Ghosh, B. K.; Solans, X. *Angew. Chem., Int. Ed. Engl.* **1994**, *33*, 2087.